# Hydrodynamics of Cloud Collisions in 2D: The Fate of Clouds in a Multi-phase Medium<sup>10</sup>

Francesco Miniati <sup>1,2,6</sup>, T. W. Jones<sup>1,7</sup>, Andrea Ferrara <sup>3,8</sup>, and Dongsu Ryu <sup>4,5,9</sup>

# ABSTRACT

We have studied head-on collisions between equal-mass, mildly supersonic HI clouds (Mach number 1.5 with respect to the background medium) through high resolution numerical simulations in two dimensions. We explore the rôle of various factors, including the radiative cooling parameter,  $\eta = \tau_{rad} / \tau_{coll}$  ( $\tau_{coll} = R_c / v_c$ ), evolutionary modifications on the cloud structure and the symmetry of the problem. Self-gravity is not included. Radiative losses are taken into account explicitly and not approximated with an isothermal adiabatic index  $\gamma \approx 1$ , which, in fact, leads to very different results. We assume a standard two-phase interstellar medium (ISM) model where clouds are characterized by a temperature  $T_c = 74K$  and number density  $n_c = 22cm^{-3}$  and are in pressure equilibrium with the surrounding warm intercloud medium (WIM), with a density contrast  $\chi = \rho_c/\rho_i = 100$ . In particular, we study collisions for the adiabatic  $(\eta \gg 1)$  and radiative  $(\eta = 0.38)$  cases which may correspond to small  $(R_c \leq 0.4pc$  for assumed WIM) or large  $(R_c \sim 1.5pc)$  clouds, respectively. In addition to a standard case of identical "non-evolved" clouds, we also consider the collision of identical clouds, "evolved" through independent motion within the intercloud gas, over one crushing time before collision. This turns out to be about the mean collision time for such clouds in the ISM. The presence of bow shocks and ram pressure from material in the cloud wake, significantly alters these interactions with respect to the standard case. In some cases, we removed the mirror symmetry from the problem by colliding initially identical clouds "evolved" to different ages before impact. In those cases the colliding

<sup>&</sup>lt;sup>1</sup>Department of Astronomy, University of Minnesota, Minneapolis, MN 55455

<sup>&</sup>lt;sup>2</sup>Dipartimento di Astronomia, Università of Firenze, 50125 Firenze, Italy

<sup>&</sup>lt;sup>3</sup>Osservatorio Astrofisico di Arcetri, 50125 Firenze, Italy

<sup>&</sup>lt;sup>4</sup>Department of Astronomy & Space Science, Chungnam National University, Daejeon 305-764, Korea

<sup>&</sup>lt;sup>5</sup>Department of Astronomy, University of Washington, Box 351580, Seattle, WA 98195-1580

<sup>&</sup>lt;sup>6</sup>e-mail: min@msi.umn.edu

<sup>&</sup>lt;sup>7</sup>e-mail: twj@astro.spa.umn.edu

<sup>&</sup>lt;sup>8</sup>e-mail: ferrara@arcetri.astro.it

<sup>&</sup>lt;sup>9</sup>e-mail: ryu@sirius.chungnam.ac.kr

 $<sup>^{10} \</sup>mbox{Published}$  in The Astrophysical Journal, December 10, 1997

clouds have different density and velocity structures, so that they provide a first insight on the behavior of more complex interactions.

In our adiabatic collisions the clouds are generally disrupted and convert their gas into the warm phase of the ISM. Although the details depend on the initial conditions, the two colliding clouds are converted into a few low density contrast ( $\chi \sim 5$ ) clumps at the end of the simulations.

By contrast, for *symmetric* radiative cases we find that the two clouds coalesce, and there are good chances for a new massive cloud to be formed. Almost all the initial kinetic energy of the two clouds is radiated away during such collisions. On the other hand, for both adiabatic and radiative collisions, symmetry breaking leads to major differences. Most importantly, asymmetric collisions have a much greater tendency to disrupt the two clouds. Portions of individual clouds may be sheared away, and instabilities along the interfaces between the clouds and with the intercloud medium are enhanced. In addition, radiative cooling is less efficient in our asymmetric interactions, so that those parts of the clouds that initially seem to merge are more likely to re-expand and fade into the warm intercloud medium. Since the majority of real cloud collisions should be asymmetric for one reason or another, we conclude that most gasdynamical diffuse cloud collisions will be disruptive, at least in the absence of significant self-gravity or of a significant magnetic field.

Subject headings: ISM: kinematics and dynamics – hydrodynamics

#### 1. Introduction

Interstellar cloud collisions (CCs hereafter) are important for the dynamical evolution of galaxies. Indeed, CCs turn out to be relevant in a large variety of important processes occurring in the interstellar medium (ISM), such as star formation, dissipation of kinetic energy and gas phase transitions. In addition, they affect the gaseous structure and the energy budget of galaxies, along with the mass spectrum of diffuse ISM clouds and their evolution.

CCs were first studied by Stone (1970a, 1970b), who was mainly concerned with the evolution of interstellar clouds and especially of their structure. In his pioneering papers he found that, despite the very high compression undergone by clouds during CCs, star formation is not enhanced. Instead, he found that colliding clouds lose mass and that large scale perturbations and internal motions (approximately radial) form within the clouds, which do not decay before the next collision. Thus, cloud hydrostatic equilibrium is severely compromised, suggesting the idea of clouds with smooth density distribution profiles instead of (clouds as) sharply bounded objects (Stone 1970b). Smith (1980) performed 1D numerical simulations and concluded that, in a dusty ISM, low Mach number (< 5) collisions are the most likely to trigger star formation. Further investigations have been carried out by Gilden (1984) and Lattanzio et al. (1985, LMPS hereafter) using 2D and 3D models, respectively. These authors studied the rôle of various parameters involved in the collisions, such as the relative size of the clouds, their masses and impact parameter. They generally concluded that CCs more often lead to disruption than to coalescence or gravitational collapse of the clouds. This again has been interpreted as evidence that the ISM should be described as a continuous distribution of gas streams and turbulent eddies (LMPS, Hunter et al., 1985). That contrasts with most dynamical models for the ISM that depict it more simply as pressure-confined neutral cold clouds (CNM) moving through a warm diffuse inter-cloud medium (WIM) (see e.g., Norman and Ferrara 1996, Vazquez-Semadeni et al. 1995 and references therein). This point is so important that further investigation of the final fate of the clouds is worthwhile. In fact, it turns out that CCs are very frequent, with a rate of about once every  $10^6 - 10^7 yr$  for individual clouds, leading to a total of  $\sim 1$  cloud collision every 100 yrin the Galaxy (Stone 1970, Spitzer 1978, Hausman 1981). Their outcome could profoundly affect the mass interchange of the various phases that are believed to exist in the ISM.

CCs may also be responsible for the buildup of the observed mass spectrum of diffuse clouds (Dickey & Garwood 1989, Solomon & Rivolo 1989, Oort 1954, Field & Saslaw 1965, Field & Hutchings 1968, Penston et al. 1969, Cowie 1980, Hausman 1982, Pumphrey & Scalo 1983, Struck-Marcell & Scalo 1984, Fleck 1996, Mousumi & Chanda 1996). Early models suggested a hierarchical scenario in which small clouds, formed in HII regions out of much larger clouds through star formation, are supposed to undergo repeated inelastic collisions and coalescence, thus engendering new clouds of larger mass (Oort 1954, Field & Saslaw 1965). Yet, an accurate model should take into account the detailed outcome of CC processes. In their model Field & Saslaw (1965) assume, for example, that each CC leads to coalescence, an uncertain assumption as discussed above and by several authors including Stone (1970a, 1970b), Hausman (1981), Gilden

(1984) and Klein, McKee & Wood (1994, KMW hereafter).

In addition, CCs are relevant for the energy budget and gaseous structure of a galaxy. Clouds are accelerated in HII regions (Field & Saslaw 1965) and by supernovae. The turbulence pressure associated with their motion determines the vertical structure of the cold neutral phase in the ISM (McKee 1990, Ferrara 1993, Norman & Ferrara 1996). The bulk motions, on the other hand, are dissipated through inelastic collisions (Spitzer 1978). It is also worthwhile to mention that the amount of energy dissipated during CCs depends on the dust content and on the metallicity of the ISM, as discussed by Ricotti, Ferrara & Miniati (1997, RFM hereafter), who determined the dependence of the elasticity of a collision on parameters such as relative cloud velocity, size, metallicity and dust-to-gas ratio. Their paper gives a useful overview of the characteristics of collisions and represents a complementary study to the present one.

The present paper is devoted to a further investigation of the consequences of CCs. In particular, we hope to determine the fate (i.e. survival, dispersal in the WIM, coalescence or fragmentation) of clouds in a two-phase ISM with canonical properties. In addition, we investigate the evolution of the cloud kinetic energy. This could be retained by the clouds as thermal energy, radiated away during the collision, or transferred to the WIM. Very recently some attention has been devoted to the hydrodynamical details that characterize the flow structure in CCs (KMW, Kimura & Tosa 1996). KMW have pointed out important instabilities that develop in the collision process. In particular, they have shown that small amplitude surface perturbations may lead to the development of the "bending mode instability" (Vishniac 1994) in the cloud shocks, which, in turn, causes the colliding material to form filamentary structures. Our work extends the KMW study by adding individual cloud evolution through the intercloud medium, before the collision. This increases the realism of the simulations by taking into account the rôle of cloud bow shocks and wakes and of nonuniform cloud structures. By colliding two clouds that have undergone different amounts of prior evolution, we introduce a simple means to relax the symmetry imposed in most previous calculations. This turns out to alter dramatically the result of the interactions in ways that extend beyond the direct influence of the bending mode. We still limit for now our attention to head-on 2D gasdynamical collisions between clouds of (initially) equal mass and Mach number.

The plan of this paper is as follows. In §2 we describe the physical problem under investigation and discuss the assumptions made. In §3 we describe the computational setup; §4 presents the main results of this study; discussion is given in §5 whereas summary and conclusions are in §6.

#### 2. Description of the problem

It is known (e.g., , Stone 1970a, 1970b, KMW) that collisions between identical homogeneous clouds are generally characterized by three main evolutionary stages as shown in Fig. 1. These are (1) a compression phase in which a shock wave forms in each cloud and propagates through

it, converting cloud kinetic energy into thermal energy. If radiative cooling is efficient, a fair fraction of this thermal energy is radiated away. Otherwise, the pressure becomes high enough to drive shocks outward from the center of the collision. At the end of the compression phase the gas is highly compressed into a thin (compared to the initial cloud size) layer, whose thickness depends on the amount of radiative losses (Fig. 1a and top panel of Fig. 3a). (2) A re-expansion phase begins when shocks generated during the collision emerge into the inter-cloud medium. During this phase a rarefaction wave propagates backwards into the clouds, forming a central low pressure and low density region (Fig. 1b and 2). Also, a fast sheet of ejecta emerges from the contact discontinuity between the merged clouds. This structure, which appears like a "jet" in 2D collisions with mirror symmetry between the clouds, is subject to Kelvin-Helmholtz instabilities (KHIs) (Fig. 3b). Also, during the re-expansion phase, a reverse shock forms and interacts with the expanding cloud material. As will be shown in §4, the qualitative and quantitative details of this phase strongly depend on the adiabaticity and symmetry of the collision. (3) There follows a collapse phase when the expansion is halted by the external surrounding medium. The pressure inside the clouds is by now much lower than in the external ambient medium, so that the cloud material is driven back toward the merged cloud core. As pointed out in the literature, during this phase Rayleigh-Taylor instabilities (RTIs) become very important, especially in disrupting the cloud surface and ablating material away from it (Fig. 1c). The details of the evolution of these properties are obviously closely related to the previous, re-expansion phase and thus depend as well on the adiabaticity of the collision. Under some circumstances it appears that one should add (4) a dispersal phase, since the original clouds may be largely converted to WIM (Fig. 1d).

In the absence of self-gravity and for Mach number high enough that Mach scaling applies (KMW) the primary parameter controlling head-on collisions between identical clouds is

$$\eta = \frac{N_{rad}}{n_c R_c},\tag{2-1}$$

where  $N_{rad}$  is the radiative cooling column density, while  $n_c$  and  $R_c$  are the cloud number density and radius, respectively. Note that this definition for  $\eta$  agrees with the one in eq. (5) of RFM; their adjustable parameter  $\alpha$  is here taken equal to unity. Thus when comparing the two sets of results our  $\eta$  should be divided by  $\alpha^{-1} \sim 3$ . If we express  $N_{rad}$  in terms of the radiative cooling time  $\tau_{rad}$ ,  $n_c$  and the individual cloud velocity  $v_c$  ( $N_{rad} = n_c v_c \tau_{rad}$ ),

$$\eta = \frac{\tau_{rad}}{R_c/v_c} = \frac{\tau_{rad}}{\tau_{coll}},\tag{2-2}$$

where, according to Spitzer (1978),

$$\tau_{rad} = \frac{3}{2} \frac{kT}{n\Lambda(n, T, Z)}. (2-3)$$

and  $\Lambda(n, T, Z)$  is the interstellar cooling function depending on number density n, temperature T, and metallicity Z. We have introduced the collision time  $\tau_{coll} = R_c/v_c$ , which is a natural timescale for CCs and is about the time over which the compression phase occurs. The collision

is adiabatic if  $\eta \gg 1$ , radiative if  $\eta \sim 1$  and isothermal if  $\eta \ll 1$ . Since according to eq. 2-3  $\tau_{rad}$  only depends on the density and temperature of the cloud (and on the metallicity, Z), then, from eq. 2-2  $\eta \propto v_c/R_c$  and we can infer that small, supersonic clouds undergo primarily adiabatic collisions, whereas interactions between large, slow clouds are mostly radiative or isothermal. Since in the adiabatic case  $\tau_{coll} \ll \tau_{rad}$ , there is not enough time for the thermal energy to be radiated away during the collision. On the other hand, in the radiative regime  $\tau_{rad} \sim \tau_{coll}$ , and during the collision a significant fraction of the energy associated with the clouds is converted into radiation. This fraction is even larger in the isothermal case.

Occasionally in calculations such as the present ones, strong radiative cooling is taken into account approximately by setting the gas adiabatic index  $\gamma \sim 1$ . That is, the flow is assumed to be inherently isothermal. This method allows much greater compression in the flow than the usual  $\gamma = 5/3$  case, an effect similar to that expected during a radiative compression. However, this approach is not appropriate for the problem at hand. As long as total energy is conserved, even a  $\gamma \sim 1$  gas will have a substantially higher pressure behind a strong shock than in front of it. That leads in the present situation to strong pressure gradients that drive gas flows out of the impact region during a collision. On the other hand, when radiative cooling is included properly, the thermal energy is removed from the interaction region (during the collision) before the re-expansion takes place, significantly reducing forces that drive gas away from that region. We carried out comparison simulations using  $\gamma \sim 1$  to approximate strong radiative cooling. They had properties very different from the properly radiatively cooled flows, actually resembling more nearly the adiabatic flows for the reasons already mentioned.

Considering weakly radiative or fully adiabatic cases, on the other hand, it is worthwhile to notice that we performed several tests with  $1.5 \le \eta \le \infty$  and did not find any substantial differences among them either in qualitative or quantitative terms. This means that even though our adiabatic simulations are characterized by  $\eta \gg 1$ , they also represent reasonably well cases with  $\eta \ge 1.5$ .

In this paper we restrict our study to head-on collision of neutral hydrogen (HI) clouds, and only consider supersonic clouds. In fact, according to Spitzer (1978), supersonic clouds should be the most common case for the ISM. We neglect for now the magnetic field. KMW and RFM included, in their calculations, a magnetic pressure term corresponding to an initially weak  $(B \sim 1 \mu G)$  magnetic field in order to limit the extraordinary compression otherwise occurring during radiative or isothermal collisions. However, a full MHD simulation was lacking. In complex flows, shear is typically more important to magnetic field behavior than compression (e.g., Frank et al. 1996, Jones et al. 1996), so full MHD may be expected to behave differently. We ignore any thermal conduction effects, as well as self-gravity in the present simulations.

We chose three different conditions for the clouds at impact, and for each investigated adiabatic and radiative flows, giving a total set of six cases. The simplest initial condition involves uniform, pressure-bound clouds, immediately adjacent and placed in motion at the start of the

simulation in an initially uniform background. Thus, these collisions take place before the clouds have formed any structure due to their motions; that is, they are "non-evolved". Although this case is not very realistic, it most closely resembles previous work (e.g., , Stone 1970a, 1970b, LMPS, KMW) and, since it produces clean demonstrations of the four stages of CCs, it is very useful as a "standard model". Next, to add some realism and to include nonuniform structures in a natural way, we also considered collisions between clouds that had evolved independently before impact. Those clouds were, otherwise, identical to the ones used in the "standard", "non-evolved" collisions. We considered two varieties of such "evolved" clouds. First we followed collisions between two clouds after each had undergone an identical evolution time (being a so-called "crushing time", defined in equation 2-4), so that the impacting clouds still had a mirror symmetry. We alternatively allowed collisions between two clouds of somewhat different evolutionary ages. Since during their evolution the clouds become increasingly irregular due to KHIs and RTIs, these last collisions involve "non-symmetric" clouds. Thus, we are able in a simple, but natural way to begin exploring the rôle of asymmetry in collisions. Properties of the clouds used in each simulation are summarized in Table 1.

The natural timescale for individual supersonic cloud evolution is the so-called "crushing time",  $\tau_{cr}$ , (e.g., KMW, Jones et al. 1994) defined as

$$\tau_{cr} = \frac{2R_c \chi^{1/2}}{v_c} = \frac{2R_c \chi^{1/2}}{Mc_{si}} = 1.3 \left(\frac{R_c}{pc}\right) \left(\frac{\chi}{100}\right)^{1/2} \left(\frac{M}{1.5}\right)^{-1} \left(\frac{c_{si}}{10km \, s^{-1}}\right)^{-1} \, Myr. \tag{2-4}$$

During an interval  $\tau_{cr}$  a cloud moving through an external medium develops a bow shock and is maximally compressed by an internal shock originating at the front part. An extended, low-pressure wake develops behind the cloud. Also on this timescale, KHIs and RTIs start to disrupt the cloud as it begins to become decelerated with respect to its background (e.g., Vietri et al. 1997). In the absence of magnetic fields, simulations show that clouds disrupt because of instabilities on timescales  $t \geq \tau_{cr}$ . Detailed discussions of the physics of individual, supersonic cloud evolution may be found in Doroshkevich & Zel'dovich (1981), Jones et al. (1994), Schiano et al. (1995), Jones et al. (1996), Vietri et al. (1997). For the clouds considered here,  $\tau_{cr} \sim 5.3 \times 10^5 yr$  in the adiabatic case ( $R_c = 0.4pc$ ) and  $\tau_{cr} \sim 2 \times 10^6 y$  in the radiative case ( $R_c = 1.5pc$ ). These are of the same order as the mean time for a cloud to have a collision in the ISM (Stone 1970, Spitzer 1978, Hausman 1981). This further supports our feeling that cloud evolution prior to the collision must be considered. In our study we begin the individual cloud evolution at  $t = -\tau_{cr}$  for "symmetric, evolved" CCs. For "non-symmetric, evolved" CCs one of the clouds begins its evolution at  $t = -1.5\tau_{cr}$  before the collision event. For these purposes, we define the collision to begin (i.e., t = 0) when the bow shocks of the two clouds osculate.

# 3. Numerical Setup

#### 3.1. The Code

We simulate the CC problem using a 2D Eulerian hydrodynamical code on a Cartesian grid. The code we used is based on an explicit "TVD", conservative finite difference scheme, second order accurate both in time and space (Harten 1983, Ryu et al. 1993). Multidimensional flows are handled by the Strang-type dimensional splitting (Strang 1968). We accounted for radiative cooling in each time step by explicitly correcting the total energy after updating hydrodynamical quantities.

Radiative losses are described generally by the following equation:

$$\frac{de}{dt} = -\mathcal{L} \tag{3-1}$$

where e is the internal energy and  $\mathcal{L} = n^2 \Lambda(n, T) - n\Gamma$  accounts for the net loss to radiation against nonadiabatic heating. The cooling term  $\mathcal{L}$  defines the cooling timescale

$$\tau_{rad} = \frac{e}{\mathcal{L}}.\tag{3-2}$$

When radiative losses are very high, as they can be during the compression phase, the cooling timescale,  $\tau_{rad}$ , is comparable to or less than the dynamical time scale which, by the Courant condition, ordinarily determines the computational time step. In this case the cooling term is labeled "stiff". There are several ways to handle stiff cooling terms (see, e.g., LeVeque 1997). One way is to choose the shorter of  $\tau_{rad}$  and the time step imposed by the Courant condition as the computational time step. However, in some situations this choice may lead to uncomfortably short computational time steps. On the other hand we could employ Strang's operator splitting approach, where the cooling is computed by multiple steps with its own time step, during one computational time step determined by the Courant condition. We chose a third approach in which eq. 3-1 is rewritten as

$$\frac{dln(e)}{dt} = -\frac{\mathcal{L}}{e} = -\frac{1}{\tau_{rad}}.$$
(3-3)

This leads to the solution between time steps j and j + 1,

$$e^{j+1} = e^j \cdot \exp\left(-\frac{\mathcal{L}\Delta t}{e^{j+1/2}}\right). \tag{3-4}$$

For this method the cooling is computed in a single step even though the cooling time scale is smaller than the dynamical time scale. The method ensures that the internal energy is always positive with the computational time step,  $\Delta t$ , determined by the Courant condition. If one uses the initial value  $e^j$  for  $e^{j+1/2}$  the radiative correction is, however, only first order accurate in time. The radiative cooling function we used,  $\Lambda(n,T)$ , includes free-free emission, recombination lines as well as collisional excitation lines with a standard solar metallicity ( $Z = Z_{\odot}$ ), whereas the heating ( $\Gamma$ ) is provided through ionization and photoionization processes and by cosmic rays (for a full description see Ferrara & Field 1994). We have neglected the effects due to dust grains considered

by RFM; this accounts for the slight difference in the ISM phase properties of our model with respect to theirs.

To allow tracking of material that was initially identified with each of the clouds we introduced a passive tracer, S, usually referred to as "color" (Xu & Stone, 1995). This quantity (actually, one for each cloud) is initially set to unity inside each cloud and zero elsewhere. It represents the fraction of material inside each cell that was originally part of one of the clouds. The evolution of the color is followed with van Leer's second-order advection scheme (van Leer 1976).

# 3.2. Grid, Boundary Conditions and Tests

In each simulation the clouds are centered on the x-axis with reflection symmetry assumed across this axis. Only the plane  $y \ge 0$  is included in the computational box. Tests with this code show that this more economical grid gives results equivalent to those obtained with a full plane. The length scale is adjusted for each case so that  $R_c = 1.0$ . In those units, the computational domain is x=[0,20] and y=[0,10]. The grid is Cartesian, so that our clouds are actually cylinders. The left, top and right boundaries are open. Reflections at these open boundaries are too small and too far away from the collision to affect the structure of the flow. Test calculations with a computational box twice as large showed no relevant differences from the results we describe below. We have explored a range of numerical resolutions, although only the computations at the highest resolution are presented here. These involve a  $1024 \times 512$  grid, which provides a resolution of 50 zones across the initial cloud radius. We have also compared our results on a uniform  $512 \times 256$  grid with the Adaptive Mesh Refinement results of KMW. Our simulations are purely hydrodynamical, while they added, for convenience a magnetic pressure (but no other magnetic effects) to limit compression behind radiative shocks. Still, for the same parameters, we obtain results consistent with theirs in terms of main hydrodynamical feature development.

### 3.3. Numerical Values, Physical Parameters and Initial Conditions

The parameters involved in the problem are quite numerous and a comprehensive study is beyond our present scope. However, since we are interested in assessing the importance of radiative losses, pre-evolution of clouds through the intercloud medium and symmetry of the problem, we have decided to restrict as much as possible the parameters' space by developing an accurate model for the multi-phase structure of the ISM, in agreement with observational data. We then adopt the most typical values for cloud and WIM physical properties as derived from such a model, hoping that they are truly representative of the ISM conditions. In the following we give an outline of model assumption.

As mentioned in §2 we consider clouds that are initially uniform and in pressure equilibrium with the inter-cloud medium. We set the initial density contrast  $\chi = n_c/n_i = 100$ , where  $n_c$  and  $n_i$ 

are the cloud and inter-cloud number densities respectively, and  $n_c = 22cm^{-3}$  ( $\Rightarrow n_i = 0.22cm^{-3}$ ); the cloud temperature is  $T_c = 74K \ (\Rightarrow T_i = 7400K)$ . This particular choice is dictated by the radiative cooling function adopted in our calculation, by pressure equilibrium assumption, and by the density contrast between the two different phases. The equilibrium thermal pressure for the ISM turns out to be  $p_{eq}/k_B = 1628 K \ cm^{-3}$ . Each cloud has an initial Mach number  $M = v_c/c_{si} = 1.5$ , where  $c_{si}$  is the sound speed in the inter-cloud medium. The adiabatic index  $\gamma = 5/3$   $(p = [\gamma - 1]e)$  is assumed throughout the calculations. For the adiabatic cases we set  $R_c = 0.4pc$ , whereas for the radiative ones,  $R_c = 1.5pc$ . With this choice of the parameters we have  $c_{si} \approx 10 km \ s^{-1}$  and  $v_c \approx 15 km \ s^{-1}$ ;  $\tau_{coll} \approx 2.6 \times 10^4 yr$  for the adiabatic cases. For the radiative cases  $\tau_{coll} \approx 9.7 \times 10^4 yr$  and the radiative cooling time inside the clouds turns out to be  $\tau_{rad} \approx 3.7 \times 10^4 \ yr$ , yielding  $\eta \approx 0.38$ . Finally, the Jeans length associated with the initial clouds is  $\lambda_j \approx 29pc \gg R_c$ . In the radiative symmetric collisions, the large density increase produced during the compression phase, causes a significant reduction of  $\lambda_i$ , which becomes comparable to, yet still larger than, the vertical size of the clouds. For this reason we have neglected self-gravity throughout our calculations (see also KMW). However in a more refined calculation, which would take into account other processes like chemical reactions or recombination processes, larger compression might be allowed making, as a result, the colliding clouds gravitationally unstable.

As explained in §2 we have allowed the described adiabatic and radiative clouds to collide under three different circumstances. For Cases 1 and 2 in Table 1, uniform clouds are placed on the grid in such a way that their initial boundaries are only 2 zones apart at t = 0.0. These are the so-called "non-evolved" cases. For Cases 3 and 4 each cloud begins on independent evolution at  $t = -\tau_{cr}$  (as appropriately determined by their properties listed in Table 1). In these cases t = 0.0 is defined as the moment when the bow shocks of the clouds osculate. For Cases 5 and 6 one of the clouds begins its independent evolution earlier, at  $t = -1.5\tau_{cr}$ . Again, the two cloud bow shocks come together at t = 0.0. Table 1 lists these details. Animations of each simulation have been posted on the World Wide Web site at the University of Minnesota.

#### 4. Results

#### 4.1. Collision of non-evolved clouds

Fig. 1 shows the four phases defined in §2 for an adiabatic collision (Case 1). At the earliest time shown (Fig. 1a),  $t = 1.5 \tau_{coll}$ , the collision is near the end of the compression phase. At the very beginning of this phase a one-dimensional analysis in the limit of strong shock can still be applied to the shocks propagating through the clouds. Theory predicts  $\rho \sim 4\rho_c$  and  $p \sim (4/3)\rho_c v_c^2$ , in very good agreement with the numerical values found (Fig. 2). The high pressure in the interaction region limits the compression and leads to a fast re-expansion. The compression phase lasts longer near the cloud centers, because the cloud column density is maximum along y = 0, and because some gas is vertically squirted out from side edges of the interaction region, right

after the beginning of the collision (Fig. 1a). The ejected material propagates through the lower density WIM, and later on develops features commonly seen in astrophysical jets. In particular this slab-jet structure shows a working surface bounded by a shock, a cocoon surrounding the jet and apparent KHIs. Nevertheless, since this gas represents a small fraction of the total mass of the clouds, it does not affect the development of the collision very much. At the end of this phase the gas is highly compressed into a layer much thinner than the initial cloud size (Fig. 1a and 2).

After  $t = 1.5 \tau_{coll}$ , as already pointed out in §2, the shocks generated within the clouds during the collision enter the WIM and allow the clouds to re-expand. Re-expansion takes place supersonically, generating a shock that, with the jet-shock, develops a nearly circularly expanding shock-structure on the x-y plane. Inside this structure a reverse shock is generated and the re-expanding cloud material begins to accumulate in a dense shell with  $\rho \sim 30\rho_i$  (Fig. 2). By t=8.2  $\tau_{coll}$  (Fig. 1b) a dense layer is well-formed and, despite its expansion, has become the region of highest density  $(\rho \sim 10 - 16\rho_i)$ . It has a nearly circular shape, except for distortions by KHIs and RTIs, which eventually form long dense  $(\rho \sim 11.5\rho_i)$  fingers. The shell expands at pretty high velocity  $(v \sim 1.1c_{si})$ . After about  $t = 12 \tau_{coll}$  the re-expansion of the shell halts, just before the reverse shock passes from the shell into the central, low-density cavity. Then the collapse of the shell begins. Fig. 1c shows the collapse phase at  $t = 37.5 \tau_{coll}$ . Eventually, the reverse shock reflects off the x-axis and rebounds. But, it is then largely disrupted by refraction in the irregular density structure of the collapsing cloud material. Large-scale vortices are generated that through KHIs and RTIs hasten the formation of complex filaments evident by  $t \sim 67.5 \tau_{coll}$  (Fig. 1d). At the end of the simulation what remains of the two clouds is a very low density central region with  $\rho$  mainly between  $2\rho_i$  and  $3.5\rho_i$  (Fig. 2), surrounded by a complex of filaments, which are mixing the original cloud material with the WIM. We deduce that, in Case 1, the likely fate of the clouds is disruption and conversion of cloud material into the WIM phase.

The analogous radiative Case 2 is shown in Fig. 3. During the compression phase (Fig. 3a) a fair fraction of the thermal energy is radiated away (Fig. 9). As a consequence, the density reaches very high values ( $\rho \sim 10^4 \rho_i$ ) and re-expansion is much slower than in Case 1. Since the re-expansion is so slow now, the reverse shock promptly penetrates all the way back to the impact surface and is reflected outwards again. This sequence, much like what happens inside a young supernova remnant (e.g., Dohm-Palmer & Jones 1996), eliminates the central low pressure region. Following this, a significant re-expansion along the initial direction of motion gives back to the merged cloud material a typical cloud-like aspect ratio. The structure undergoes some vertical expansion too, but the most prominent feature in this direction is a thin jet propagating along the symmetry plane of the collision. This is shown in Fig. 3. At  $t = 9 \tau_{coll}$  (Fig. 3b), almost all the cloud gas is still in a core with high density ( $\rho \sim 580\rho_i$ ), surrounded by lower density material with  $\rho$  ranging between 200 and  $450\rho_i$ , and expanding at a very low speed. A comparison of Fig. 3b with Fig. 1b shows clearly that the size of the re-expanded cloud is much larger in the adiabatic case than in the radiative one. As a consequence, in the radiative case the slab-jet structure is much more distinct. For Case 2 the simulation ends at  $t = 37.5 \tau_{coll}$ . We deduce that

in Case 2 the likely fate of clouds is coalescence. The apparently coalesced clouds have evolved into an almost circular object of radius  $\sim 2R_c$  with densities ranging between about  $20\rho_i$  in the inner part and  $70\rho_i$  at the surface. Its total mass is  $M_{tot} \simeq 0.84 \times 2 \times M_c$ , where  $M_c$  is the initial cloud mass, showing a high efficiency (84%) for the buildup mass mechanism. The edge of the newly formed object is sharply bounded, but shows clear signs of KHIs. However, because of the high density of its external layer, KHIs will become effective on a timescale much longer than in the adiabatic case. The expansion velocity inside the merged cloud at the end is small; namely a few  $\times 10^{-2}c_{si}$ . The net radiative cooling is positive (which means on balance that the gas is losing thermal energy) in the outer, denser part of the merged clouds, and negative (which means that the gas is being heated up by the background radiation and cosmic rays) in the inner more diffuse region, although in both cases the energy gains or losses are not very significant. There is a small outward-facing pressure gradient within the cloud concentration, so eventual collapse seems likely. Although coalescence seems likely in the near-term, the final fate of the cloud is unclear. KMW suggest that the cloud will expand and contract multiple times until pressure and thermal equilibrium are reached, developing filamentary structures along the x-axis in the process. It might also be possible that the lower pressure inside the cloud induces contraction followed by a sufficient increase in the density to turn the cooling function positive. In that case the extra pressure due to in-fall could be radiated away and the original cloud density, for which radiative equilibrium holds, might be approached. In addition, because of the highly dense external layer around the newly formed structure, we do not expect in the radiative case that RTIs will be as disruptive during the collapse phase as for the adiabatic case.

#### 4.2. Collision of evolved clouds: symmetric cases

Fig. 4a shows the initial conditions for the adiabatic collision of two evolved clouds (Case 3). At t=0, when the cloud bow shocks just touch and each cloud has evolved through one crushing time, the density changes smoothly through the clouds, ranging from  $10\rho_i$ , at the back, to 150  $\rho_i$ at the front part. The x-component of the velocity follows the same pattern, being higher at the front of the cloud than at the rear, although the range of this variable is much smaller (e.g., Jones et al. 1994). On average the clouds have an individual speed corresponding to a Mach number, M=1.35, relative to the WIM. There are a number of differences introduced into the interaction between the clouds by allowing for prior evolution. The most important are the presence of bow shocks and incoming gas motions within each cloud wake once the clouds collide. After the approaching clouds encounter each other's bow shock, reverse shocks (which act as secondary bow shocks) are generated. In the adiabatic interaction (Case 3) these shocks substantially affect the clouds. In fact at  $t = 2.2 \tau_{coll}$ , right before the cloud bodies encounter the bow shocks, their x-width  $\ell \sim 1.5R_c$  and  $\rho_{max} \sim 150$ , but at  $t = 3 \tau_{coll}$ , after the bow shock-cloud collision begins,  $\rho \sim 250 \rho_i$  (  $\rho_{max} \sim 260 \rho_i$ ) and  $\ell \sim 1.2 R_c$ . There is further compression so that at  $t \sim 3.8 \tau_{coll}$ , right before the cloud bodies impact each other,  $\rho \sim 380\rho_i$  in the compressed front layer, and  $\ell \sim R_c$  (Fig. 4b). So, the maximum compression reached during the collision (  $t \sim 4.5 \tau_{coll}$ )

 $(\rho_{max} \sim 1200\rho_i)$  is much higher in Case 3 than in Case 1, although the pressure enhancement is about the same, and both collisions are adiabatic. If the clouds were self-gravitating, such differences might become important to the possibility for triggering star formation out of such collisions. On the other hand, the jet-like and the thin shell structures develop in roughly the same pattern as for Case 1. By comparison to the non-evolved collision, however, more cloud material remains in a core structure, almost to the re-expansion phase. This is evident in Fig. 1b. at  $t = 11.2 \tau_{coll}$ , when contrasted with Fig. 4c. The same comparison also shows that the shell structure in Case 3 is more irregular than in Case 1. This is in fact due to the lower density of the shell of Case 3, which allows a quicker development of RTIs and KHIs. By the time shown in Fig. 1c expansion along the x-axis has been reduced compared to the y-direction. That results from the interaction between the expanding cloud material and inflowing WIM within the wakes of the two clouds. The ram pressure of the wake flows is strong enough to affect significantly the expansion along this path. Indeed at  $t \sim 15 \tau_{coll}$  a standing, reverse shock is well formed and deflects the expanding cloud material away from the x-axis. This in turn becomes strongly sheared and filamentary due to KHIs. A substantial fraction of the cloud material is ejected so that it cannot join the collapse. The shock structures in this case are very complex, since they involve interactions with the pre-existing bow shocks and tail shocks and a generally more complex density and pressure structure as the collision begins. Nevertheless, as our simulation of Case 3 ends ( $t = 22.5 \tau_{coll}$ ), the dominant, irregular shell structure resembles qualitatively that in Case 1. Subsequent evolution in Case 3 should follow a pattern similar to that in the analogous non-evolved Case 1. In particular we expect disruption of the clouds in both cases.

In the radiative evolved case (Case 4) the individual clouds show a similar qualitative structure as in Case 3, but now their compression due to initial motion through the inter-cloud medium is much higher ( $\rho_{max} \sim 1400 \rho_i$ ). The additional compression results from enhanced radiative cooling induced by the shock compression within the cloud. We note that the bow-shock compression phase that was important to Case 3 turns out not to produce a very significant effect for Case 4. That is because the compression brought on by radiative losses prior to the encounter is already very large. In addition, since the speed at which the bow shock penetrates each cloud scales inversely with the square root of density, in this case the bow shocks barely penetrate into the clouds bodies before they collide, producing only little pre-compression with respect to the adiabatic case. As a result, the compression reached during the collision is only slightly higher (  $\rho_{max} \sim 4 \times 10^4 \rho_i$ ) than in the non-evolved case (Case 2). The re-expansion phase in Case 4 follows pretty much the same pattern as in Case 2, except that now it is substantially slowed down in some directions by the action of the wakes behind each cloud, as we noted also for Case 3. In fact, as shown in Fig. 5, by the end of this simulation (  $t = 22.5 \tau_{coll}$ ) the clouds have merged into a dense structure of size  $\sim 2R_c$ , which is 2/3 of the size of the merged core in Case 2. Expansion in the y-direction is relatively free and leads to a KH unstable jet as in the other symmetric collisions. However, re-expansion along the x-axis is strongly inhibited by inflowing wake material, so that the velocity of expansion along the x-axis is only about 1/3 as large, compared to Case 1. As a result the expanding gas collects in a high density cloud "rim" ( $\rho \sim 400\rho_i$ ,  $\rho_{max} \sim 440\rho_i$ ). The

wake material forms a standing, outward facing, "accretion shock" outside the cloud structure. Examination of the color variable shows a very good correspondence between the high density material visible in Fig. 5 and cloud material. Thus, the figure shows that wake material, once it impinges on the cloud, joins the outflow of cloud material in the y-direction. In fact, it appears that the inflowing wake material and associated shocks are responsible for driving the vertical outflow of cloud material along the jet and for producing the KHIs that have generated the large eddies evident in Fig. 5. In the inner cloud the density ranges between 100 and 200  $\rho_i$ , which is higher by almost a factor 2 with respect to the non-evolved case. Even though there is a weak pressure gradient pushing vertically in the central condensation, it seems very likely that in an extension of this simulation the main core of the merged clouds would remain intact. So, we judge these clouds to be coalesced.

# 4.3. Collision of evolved clouds: asymmetric cases

As mentioned earlier we chose a simple, but natural way to explore symmetry breaking in the collisions just discussed. That is, we collided clouds that were identical when set into motion, but which were differently evolved at impact. On a timescale  $\sim \tau_{cr}$  the compression substantially deforms the clouds, while KHIs and RTIs will produce irregular cloud boundaries. Since those features are highly time dependent, two clouds of even slightly different dynamical ages will lack mirror symmetry. In our asymmetric simulations one cloud (C1 hereafter, and on the left) was aged by 1  $\tau_{cr}$  and the other (C2 hereafter, and on the right) by 1.5  $\tau_{cr}$  as their bow shocks came in contact at t = 0.0. The older cloud had in general a denser front part and a smaller velocity at impact (Jones et al. 1994). However the aspect ratio (length to height ratio) developed by the cloud during its motion through the WIM is strongly related to the adiabaticity of the gas. Indeed it increases in the adiabatic case, but decreases in the radiative one, so that the radiative cloud grows denser and more compact as it evolves (Vietri et al. 1997). This turns out to have a major impact on the survival of clouds in asymmetric CCs. As in the previous evolved cases, the two clouds undergo bow shock-compression before colliding bodily. In the asymmetric interactions the clouds have different speeds and shapes, and are located at different distances from their bow shocks. As a result they no longer experience compression simultaneously. In addition, since C2's bow shock is weaker than C1's, bow-shock compression for C2 turns out to be stronger than for C1. In the adiabatic Case 5, right before the direct collision, C1 has  $\rho \sim 300\rho_i$  and  $\ell \sim R_c$  and C2 has  $\rho \sim 370\rho_i$  and  $\ell \sim 0.6R_c$ . The compression phase is shorter than in Cases 1 - 4, and not all of the kinetic energy is converted into thermal energy (Fig. 8). After the collision, the younger, more compact cloud C1, maintains its identity longer than C2. As shown in Fig. 6, at t = 8.2 $\tau_{coll}$  C1 still has a dense core with  $\rho \sim 70\rho_i$  surrounded by a layer with  $\rho \sim 40\rho_i$ . By contrast, C2 is being stretched and torn apart and, soon after, is mostly converted into the WIM. Nevertheless C1 is undergoing rapid re-expansion too and, at  $t = 13.5 \tau_{coll}$ , the density is lower than 15  $\rho_i$ everywhere. Although it is much more irregular than Cases 1 or 3, in Case 5 we can still recognize a clear pattern in the evolution of the re-expansion phase, with the formation of an expanding

shock wave along with a reverse shock and a low density shell, heavily affected by KHIs and RTIs. So, at the end of the second, re-expansion phase, part of the cloud gas has already been converted into WIM, whereas the remaining part is forming an irregular filamentary structure with  $\rho$  ranging between 5 and  $10\rho_i$ . As in the symmetric-evolved collisions, the interaction between re-expanding cloud material and inflowing wake gas significantly influences the expansion. As for Case 3 the wake confines expansion along the x-axis through a standing, inward-facing shock. Also, as in Case 3, the expanding cloud material is deflected around the wake in a strongly sheared manner. The broken symmetry in Case 5 allows C2 material to expand much more easily, however, because its greater y-extent at impact effectively "launches" it over the wake of C1. In addition, since C2 has a lower column density just above the x-axis, it recoils in response to the collision. Thus, a substantial fraction of C2 passes over its own wake after the collision. Those effects add considerably to the disruption of cloud material into filaments and probably hastens its dispersal into the WIM. The resulting flow is very complex and highly vortical. So, we expect the collapse phase to be very ineffective at collecting together material into new clouds. Thus, this case seems clearly much more disruptive that any of the previous ones.

On the other hand, the radiative Case 6 is characterized by completely new features. At t = 2.2  $\tau_{coll}$  the region between the two shocks formed by the collision, appears to be strongly distorted, resembling the structure that develops during the "bending mode instability" (KMW, Vishniac 1994, Hunter et al. 1986). As shown in Fig. 7a, at  $t=3 \tau_{coll}$  the layer between the two shocks has grown more corrugated and the front parts of the clouds are following the same pattern. Although the bending mode is unstable, the disruption of the impact surface is primarily due to the gross irregularities of clouds' shape, which dominate the determination of the evolution of the structure of the flow. Fig. 7a shows also that the upper part of the left (C1) cloud is about to break off and pass over the other cloud (C2), carrying some of C2's gas with it. As already pointed out, unlike the adiabatic case, in the radiative case the older cloud C2 has a more compact structure, which makes it more solid and more resistant to the collision than C1. At t = 9  $\tau_{coll}$  (Fig. 7b), the material from C1 passing over the top of C2 has expanded again into a distinct cloudlet, with density ranging from  $\rho \sim 100\rho_i$  at the front, to  $\rho \sim 5\rho_i$  at the tail, and with still slightly supersonic velocity ( $v_x \geq c_{si}$ ). Subsequently, that cloudlet becomes strongly decelerated and suffers KHI- and RTI- induced destruction, as seen previously for individual clouds (e.g., Jones et al. 1994). Although the cloudlet leaves our grid before it is destroyed, it seems fairly clear that it will dissolve into the WIM. The wake of the cloudlet is still visible on the far right side in Fig. 7c. On the other hand the core of C2, which by  $t=3 \tau_{coll}$  has a very long tail and a dense, but distorted front, passes through the remaining part of C1, emerging after  $t \approx 7.5 \tau_{coll}$  with the main body of C2 accreted. This outcome resembles those one would expect in collisions of two clouds of quite different sizes and densities. It shows that the smaller and denser cloud is able to pass through the larger and more diffuse one, sweeping its gas and finally breaking it up into two major pieces (Gilden 1984, Kimura & Tosa 1996). In these calculations we show that the same fate can actually occur when two clouds with approximately the same initial characteristics but with slightly different morphologies collide.

As in the other collisions between clouds that are followed by wakes, an "accretion" shock forms to the right of C2. However, it is driven off the grid to the right before the simulation ends. The interaction is dominated in this case by the high concentration of material in C1.

The merged remnant of C1 and C2 that was formed by  $t=7.5~\tau_{coll}$  has by the end of the simulation,  $t=30~\tau_{coll}$ , evolved into non uniform filamentary structures, characterized by irregular motion (Fig. 7c). Very little mixing between the two original clouds has actually taken place; rather one has passed through the other. On the other hand, considerable entrainment of WIM gas has taken place through the action of eddies generated during the collision. The higher density features apparent on the left and top perimeter of the main cloud visible in Fig. 7c are, in fact, the remnant merged cores of the original clouds, whereas the rest of the main cloud at this late time contains a strong mix of entrained material, or has been ejected from the grid. At this time the main cloud is being slowly stretched along the x-axis ( $v_x \sim 0.1c_{si}$  at the edges), while large eddies on the top and downward pointing pressure forces are being effective at reducing its height. It seems likely that the single dense region visible in Fig. 7c will be bisected into two before too long. The final outcome may be two distinct clouds formed largely from material originally in C2, which was the more compact of the original pair. Thus the outcome is completely different from that of Cases 2 and 4 and we conclude that the two clouds are destroyed by the collision and converted into several filamentary structures.

#### 5. Discussion

We have investigated for the six cases summarized in Table 1 the collision of diffuse HI clouds in a multi-phase medium. Our objective is to understand such issues as the likely fate of clouds after collisions, including the conditions for coalescence and the fraction of the initial kinetic energy radiated away. In the previous section we outlined the basic dynamical evolution of each collision and the ultimate fate of the clouds. It was clear from those examples that the fate of colliding clouds depends strongly on the symmetry of the interaction and also on the degree to which the initial kinetic energy is radiated away before the clouds begin their re-expansion. To clarify and expand on those issues we now review the main points, separately for the adiabatic and radiative cases.

#### 5.1. Adiabatic Cases

Adiabatic collisions generally appear to result in cloud disruption, with most of the gas converted into the WIM phase. This point is made clearer in Fig. 8, which shows a plot of various properties characterizing individual clouds involved in adiabatic collisions. In particular, using the color variables, we can follow the kinetic and thermal energies of each cloud, normalized to the initial cloud total energy, as well as the center-of-mass coordinates  $x_{cm}$  and  $y_{cm}$  for each cloud

relative to the point of first contact (see Jones et al. 1996 for a mathematical definition of  $x_{cm}$  and  $y_{cm}$ ). From a comparison of panels (a) and (b) in Fig. 8, we see that in all adiabatic Cases 1, 3 and 5 the kinetic energy of the clouds  $E_{kin} = 1/2M_cv_c^2$  is initially converted mostly into thermal energy  $E_{ther} = pV/(\gamma - 1)$  during the compression phase, through the action of the main, outward moving shocks as they pass through the cloud bodies. That stage is immediate for the "nonevolved" collision, but is delayed, of course, for the "evolved" cases, since t=0 corresponds to the moment when the bow shocks touch, rather than when the clouds first touch. During the re-expansion phase, some of this thermal energy is converted back into kinetic form, since the rapid expansion of the "blast wave" into the WIM, reduces the pressure around the merged clouds. But, because the cloud shocks have generated entropy, the cloud gas has substantially more thermal energy at the end of each simulation than at the start, despite considerable volume expansion. This effect enhances the tendency for the cloud material to be converted into the WIM phase following the collision. Also, these plots show that the normalized kinetic energy decreases gradually with time; this is due to the irreversible work done by the expanding gas on the surrounding background. A similar trend was observed in the 3D simulations of two colliding gas streams by Lee et al. (1996). It is important to notice that at late times (  $t \ge 8 \tau_{coll}$ ) some energy decrease is also due to escape of matter from the computational domain, particularly the top. The center-of-mass positions provide a quantitative measure of this expansion as shown in panels (c) and (d). In particular, note for Case 1 that the maximum in  $y_{cm}$  around  $t \geq 8 \tau_{coll}$  corresponds to the time when the dense shell reaches the top of the grid. After that time  $y_{cm}$  represents only mass the remaining within the grid. Panel (c) also illustrates quantitatively how cloud material in the symmetric collisions is more efficiently removed from the central interaction region than in the asymmetric case. Notice for Case 5 that some cloud material remained in the interaction region interior. In panel (d) we also see the clear difference in y-expansion of the individual clouds in the asymmetric Case 5. The more evolved cloud, C2, which begins the simulation having a greater height and lower column density along central impact axis, is obviously disrupted by this measure. The more compact cloud, C1, remains compact in this dimension, on the other hand.

#### 5.2. Radiative cases

In the radiative cases, as long as the initial geometry is symmetric, the two colliding clouds merge and it seems likely that the conditions for a new massive cloud to form do exist. As shown in Fig. 9, the kinetic energy of the two clouds is converted into thermal energy and soon radiated away. In deed, unlike the adiabatic cases, after the compression phase there is no re-enhancement of the kinetic energy, as is shown by a comparison of panels (c) and (d) in Fig. 9 and 8. As a result the re-expansion of the gas is much reduced with respect to the adiabatic case. At the end of the evolution the thermal energy of the clouds has increased, due to heating processes occurring during the re-expansion phase (Fig. 9). Also, in the evolved (symmetric) cases, the density at the compressed layer formed during the collision is higher than in the non-evolved case and this could be important for triggering star formation processes. Furthermore, the wakes developed during

the cloud evolution limit the re-expansion, so that after the collision in Case 2 the merged clouds end up forming a smaller and denser region. In cases where self-gravity is dynamically important, the wake effect could play a fundamental rôle, reducing the expansion velocity of the material below the escape threshold, thus making it possible for the two clouds to build up a new larger, gravitationally bound structure (see, also, Dinge (1997) for similar behavior in a single, moving, self-gravitating cloud).

The outcome of CCs is very different for the asymmetric, i.e. differently evolved clouds, even though our collisions all involve clouds of equal mass and head-on collisions. In this case we obtain fragmentation of the "younger" cloud and the formation of a small expanding cloudlet eventually dissolving into the WIM. As shown in Fig. 9, in this case only part of the initial kinetic energy is radiated away during the collision. As a result, the remainder of the merged cloud material re-expands and, through interaction with the wake flow, becomes concentrated into dense clumps. At the end most of the cloud material has been converted into WIM, its directed kinetic energy partly being lost to radiation, partly to turbulent gas motion. KMW have shown that by slightly perturbing the surface of one of the two colliding clouds, the bending mode instability causes fragmentation rather than coalescence. In our study the asymmetry in the problem is due to a slight difference in the evolutionary ages of the clouds  $(0.5 \tau_{cr})$ . As already pointed out, its effect is comparable to that of an off-center collision. That is, the mass and momentum of the two clouds at impact have significantly different y distributions. Those structural differences of the clouds make the outcome of the collision very different from the symmetric cases. From this fact we conclude that supersonic radiative collisions of clouds with the same gross characteristics (mass, speed and structure), but without high symmetry, are disruptive and generate irregular filamentary clumps. On the other hand previous results show that collisions of clouds with major structure differences (density, size), are likely to be disruptive as well (Hausman 1981, Gilden 1984, Kimura & Tosa 1996, RFM). Our results support this. In addition, our results show that the adiabatic case, which applies to small clouds, will be highly disruptive, even if the clouds are identical and the collision head-on. Also, as pointed out below, off-center collisions, which are the most common, certainly are very unlikely to produce coalescence of clouds, at least for non-self-gravitating objects.

These results have an important impact on the ISM of galaxies. In general, supersonic, gasdynamical CCs tend to be disruptive, so that any model to explain cloud evolution and mass spectrum has to take these findings into account. If colliding clouds are sufficiently electrically conductive, then the presence of a large-scale magnetic field may play an important dynamical rôle in the interaction. It is not obvious, however, that our main conclusion will be altered. We have fully MHD simulations underway that will address that point in a separate report.

It is worthwhile to mention that our asymmetric calculations can provide some insights for off-center collisions as well, at least for those with small impact parameter ( $b \ll R_c$ ). In fact, with regard to survival of the clouds, the most important implication for small impact parameter off-center collisions is probably asymmetry. For these cases the results of our asymmetric calculations may apply as a guide, at least for clouds of comparable mass. However, when the

impact parameter  $b \sim R_c$ , only part of the cloud is involved in the collision and our calculations are not appropriate anymore. LMPS have investigated off-center, isothermal collisions for very massive clouds, including gravity in their calculations. They show that, for high relative velocity, the colliding parts of the clouds soon re-expand and disperse after the compression phase, whereas the outer parts (which do not get involved in the collision) proceed unhindered and form two new small clouds. On the other hand, for low relative velocity, the colliding clouds coalesce, whereas the outer gas motion is deflected into a circular pattern. As a result rotating bound systems and bars form. For smaller non-self-gravitating clouds, we think that, in addition to the relative velocity, the adiabaticity is a key parameter. If  $b \leq R_c$  the collision can probably be classified in similar terms to a highly asymmetric one. On the other hand, if  $b \geq R_c$ , the LMPS calculations suggested that the outer part of the clouds are torn apart during the collision. For an adiabatic collision, pressure waves in the remaining clouds generated during the encounter might be able to make the clouds expand and disperse into the WIM. However, in a strongly radiative encounter these waves could be damped away by radiation and the cloud cores might survive, although the clouds themselves would turn out quite distorted Finally, if  $b \sim 2R_c$ , the collision will produce only minor perturbations on the cloud structures.

Real clouds are, of course, three dimensional. CC three-dimensional calculations have been performed by Hausman (1981), LMPS and Lattanzio & Henriksen (1988, LH hereinafter); these authors, using a smoothed particle hydrodynamics code, investigate on the effects of several parameters (relative velocity, cloud mass ratio, impact parameter and so on) on coalescence. Hausman's calculations are strongly affected by the limitations of his computational means. In particular he used a resolution as low as 100 particles per cloud, and his calculations show unphysical particle interpenetration. For this reason, for example, in his run 1, Hausman finds a ratio  $p_{max}/p_{ext}$  of only 3.55, much less than 50 as found by LMPS for the same case. As a result, little conversion of kinetic energy into thermal energy takes place; it is probably for this reason that, in most of his runs, Hausman finds that the cooling is efficient enough to ensure isothermality (Hausman 1981). Since the set of cases studied by Hausman is very similar to that presented by LMPS, we will neglect to go in more details about his results. LMPS employed a better version of smoothed particle hydrodynamics code (Monaghan & Lattanzio 1985), and higher resolution ( $\sim 2000$  particles per cloud). We have already summarized their results regarding off-center collisions. They also found that symmetric head-on collisions generate a single rapidly re-expanding or collapsing cloud depending on whether the initial clouds are gravitationally stable or unstable respectively. In asymmetric (but still head-on) cases however, they concluded that even when a cloud is marginally stable to gravitational collapse, the collision with a smaller cloud (ratio of masses larger than 2.5; their clouds had the same density), does not initiate the instability. Finally LH further investigated this problem showing how spin and orbital angular momentum are important in determining the outcome of CCs. The accuracy of these results, although useful and to some extent in agreement with previously cited works and our own, is still limited by low resolution ( $\sim 2000$ , 3000 particles) and some assumptions which are not always appropriate. Some of these were mentioned by the authors themselves. In addition, based

on Hausman (1981) results, both LMPS abd LH assumed isothermal clouds, using  $\gamma=1$ ; but as already pointed out, this approach is not correct because of the fundamental dynamical rôle played in the re-expansion phase by thermal energy stored during the compression phase. That aspect is apparent in our results. In our radiative head-on symmetric simulations, which allow for a release of energy through radiative processes, the collisions produce a new merged stable cloud instead of a rapidly re-expanding cloud as found by LMPS. Also LMPS and LH do not include in their calculations an intercloud medium. However, as we have noted, the interaction of cloud material with the intercloud gas, particularly with shocks and cloud wakes, significantly affects the evolution of the collision.

Useful insights about how an additional degree of freedom in this problem might modify 2D results may be provided by 3D studies of some related problems. For example, Xu & Stone (1995) examined the evolution in 3D of a gas cloud overrun by a plane shock. They found behaviors qualitatively consistent with 2D simulations of that problem (e.g., Bedogni & Woodward 1990; Jones & Kang 1993; KMW). In many respects a shocked cloud is similar to a supersonic cloud in its evolution (Jones et al. 1994). Lee et al. (1996) have carried out a 3D study of two colliding gas streams. That is similar in some ways to collisions between clouds. They found, as we do for adiabatic collisions, that the bulk of the kinetic energy is converted into thermal pressure, and that this causes the colliding material to expand as it drives a shock into the ambient medium. Generally, the extra dimension will allow more complex motions to develop, and some considerations will depend quantitatively on the third dimension, but we see no evidence in the existing literature that the general conclusions of the present work will be invalidated when it is included.

### 6. Conclusions & Summary

To summarize, in this paper we have found the following results for the gasdynamical collisions between two mildly supersonic interstellar clouds,  $M \ge 1.5$ , of comparable mass:

- 1. Supersonic CCs are most often disruptive. In particular adiabatic collisions, which involve small clouds ( $R_c < 0.4pc$ , for the standard WIM parameters assumed in our calculations), turn out always to be disruptive.
- 2. For completely symmetric collisions, strong radiative energy losses can, however, lead to coalescence of the two clouds. In fact emission of radiation reduces the thermal energy stored during the compression phase, preventing a vigorous pressure driven re-expansion.
- 3. Asymmetry in the clouds at impact greatly enhances the tendency for clouds to be disrupted during the interaction, even when radiative cooling is strong. This is true even for a very modest asymmetry. In the adiabatic, asymmetric case the clouds are almost immediately dispersed in the WIM. In the radiative case new filamentary structures are produced out of

the initial cloud material.

4. Future numerical work should not neglect the importance of allowing the clouds to develop a self-consistent structure, especially bow shocks and wakes, since these features strongly influence the interaction and add important hydrodynamical features. In particular, bow shock interaction of the colliding clouds produces higher compression, particularly in the adiabatic case. On the other hand the wakes behind the clouds reduce the re-expansion along the x-axis, increasing the probability for coalescence.

FM devotes his efforts in this work, to the memory of his friend, Leonardo Muzzi, young artist of deep perspective, who inspired his way of studying science. This work by TWJ and FM was supported in part by the NSF through grants AST-9318959 and INT-9511654 and by the University of Minnesota Supercomputer Institute. The work by DR was supported in part by Seoam Scholarship Foundation. AF acknowledges hospitality of University of Minnesota where this work started.

#### REFERENCES

Bedogni, R. & Woodward P. 1990, A&A, 231, 481

Cowie, L.L. 1980, ApJ, 236, 868

Dickey, J. M., & Garwood, R. W. 1989, ApJ, 341, 201

Dinge, D. 1997, ApJ, 479, 792

Dohm-Palmer, R. C. & Jones, T. W. 1996, ApJ, 471, 279

Doroshkevich, A.G., Zel'dovich, Ya.B., 1981, Soviet-Phys.-JETP, 53,405

Ferrara, A. 1993, ApJ, 407, 157

Ferrara, A., & Field, G.B., 1994, ApJ, 423, 665

Field, G.B., & Hutchins, J. 1968, ApJ, 153, 737

Field, G.B., & Saslaw, W.C. 1965, ApJ, 142, 568

Fleck, R. C. 1996, ApJ, 458, 739

Frank, A, Jones, T. W., Ryu, D. & Gaalaas, J. B. 1996, ApJ, 460, 777

Gilden, D.L. 1984, ApJ, 279, 335

Harten, A., 1983, J. Comp. Phys., 49, 357

Hausman, M.A. 1981, ApJ, 245, 72

Hausman, M.A. 1982, ApJ, 261, 532

Hunter, J. H., Sandford II, M. T., Whitaker, R. W., Klein, R. I. 1986, ApJ, 305, 309r

Jones, T. W., & Kang, H. 1993, ApJ, 402, 560

Jones, T. W., Kang, H., & Tregillis I. L. 1994, ApJ, 432, 194

Jones, T. W., Ryu, D., & Tregillis I. L. 1996, ApJ, 473, 365

Kimura, T., & Tosa, M. 1996, A&A, 308, 979

Klein, R.I., McKee, C.F., & Woods, D.T. 1995, in The Physics of Interstellar Medium and Intergalactic Medium, ed. A.Ferrara, C.F.McKee, C. Heiles, & Shapiro, P. R.: ASP, 80, 366 (KMW)

Lattanzio, J. C., & Henriksen, R. N. 1988, MNRAS, 232, 565 (LH)

Lattanzio, J. C., Monaghan, J. J., Pongracic, H. & Schwarz, M. P. 1985, MNRAS, 215, 125 (LMPS)

Lee, H., Kang, H. & Ryu, D. 1996, ApJ, 464, 131

LeVeque, R. J., 1997, Computational Methods in Astrophysical Fluid Flows, 27th Saas-Fee Advanced Course Lecture Notes (Springer: Berlin), in press

McKee, C.F. 1990, in "The Evolution of the Interstellar Medium", ed. L.Blitz: ASP, 12, 3

Monaghan, J. J. & Lattanzio, J. C., 1985, A&A, 149, 135

Mousumi, D. & Chanda, J. J. 1996, ApJ, 462, 309

Norman, C. A. & Ferrara, A. 1996, ApJ, 467, 280

Oort, J.H. 1954, B.A.N., 12, 177

Penston, M.V., Munday, V.A., Stickland, D.J., & Penston, M.J. 1969, MNRAS142, 355

Pumphrey, W.A., & Scalo, J.M. 1983, ApJ, 269, 531

Ricotti, M., Ferrara, A. & Miniati, F. 1997, ApJ, in press (astro-ph/9702143) (RFM)

Ryu, D., Ostriker, J. P., Kang, H. & Cen, R., 1993, ApJ, 414, 1

Schiano, A. V. R., Christiansen, W. A. & Knerr, J. M. 1995, ApJ, 439, 237

Smith, J. 1980, ApJ, 238, 842

Solomon, P. M., & Rivolo, A. R. 1989, ApJ, 339, 919

Spitzer, L. 1978, Physical Processes in the Interstellar Medium, (New York: Wiley)

Stone, M.E. 1970a, ApJ, 159, 277

Stone, M.E. 1970b, ApJ, 159, 293

Strang, G. 1968, SIAM J. Num. Anal., 5, 506

Struck-Marcell, C., & Scalo, J.M. 1984, ApJ, 277, 132

Vazquez-Semadeni, E., Passot, T., & Pouquet, A. 1995, ApJ, 441, 702

Vietri, M., Ferrara, A. & Miniati, F., 1997, ApJ, 483, 262

Vishniac, E. T. 1994, ApJ, 428, 186

Xu, J. & Stone, J. M. 1995, ApJ, 454, 172

van Leer, B. 1976, J. Comput. Phys., 23, 276

This preprint was prepared with the AAS LATEX macros v4.0.

Table 1. Summary of 2D-HD Cloud Collisions Simulations

Case <sup>a</sup>	$\eta^{ m b}$	$R_c$	$\tau_{coll} = R_c/v_c$	$\tau_{cr} = 2R_c \sqrt{\chi}/v_c$	$M_r^{\ c}$	Clouds ages <sup>d</sup>	End Time <sup>e</sup>
1	adiabatic	$0.4~\mathrm{pc}$	$2.6 \times 10^4 y$	$5.3 \times 10^5 y$	3	$0 \tau_{cr}$ - $0 \tau_{cr}$	$67.5 \ \tau_{coll}$
2	0.38	$1.5~\mathrm{pc}$	$9.7 \times 10^4 y$	$2.0 \times 10^{6} y$	3	$0 \tau_{cr}$ - $0 \tau_{cr}$	$37.5 \ \tau_{coll}$
3	adiabatic	$0.4~\mathrm{pc}$	$2.6 \times 10^4 y$	$5.3 \times 10^5 y$	2.7	$1 \tau_{cr}$ - $1 \tau_{cr}$	$22.5 \ \tau_{coll}$
4	0.38	$1.5~\mathrm{pc}$	$9.7 \times 10^4 y$	$2.0 \times 10^{6} y$	2.8	$1 \tau_{cr}$ - $1 \tau_{cr}$	$22.5 \ \tau_{coll}$
5	adiabatic	$0.4~\mathrm{pc}$	$2.6 \times 10^4 y$	$5.3 \times 10^5 y$	2.4	$1 \tau_{cr}$ - $1.5 \tau_{cr}$	$22.5 \ \tau_{coll}$
6	0.38	$1.5~\rm pc$	$9.7 \times 10^4 y$	$2.0 \times 10^{6} y$	2.7	1 $\tau_{cr}$ - 1.5 $\tau_{cr}$	$30.0 \ \tau_{coll}$

<sup>&</sup>lt;sup>a</sup>All models have used  $\gamma = 5/3$ ,  $\chi = \rho_c/\rho_i = 100$ , equilibrium pressure  $p_{eq}/k_B = 1628~K~cm^{-3}$ . Also, at equilibrium, we have  $T_i = 7400K$  and  $n_i = 0.22~cm^{-3}$  for the inter-cloud medium and  $T_c = 74K$  and  $n_c = 22~cm^{-3}$  inside the clouds. Furthermore, all the computations were carried out on a rectangular grid with size  $N_x = 2N_y = 1024$  corresponding to a resolution of 50 zones through the cloud radius. Left, top and right boundaries are free whereas reflection is assumed at the bottom.

 $<sup>^{\</sup>mathrm{b}}\eta = \tau_{rad}/\ \tau_{coll}$ 

<sup>&</sup>lt;sup>c</sup>This is the *relative* Mach number and is referred to the inter-cloud sound speed,  $c_{si} \simeq 10 km \ s^{-1}$ .

<sup>&</sup>lt;sup>d</sup>The left and right hand columns refer to the left and right hand clouds, C1 and C2, respectively.

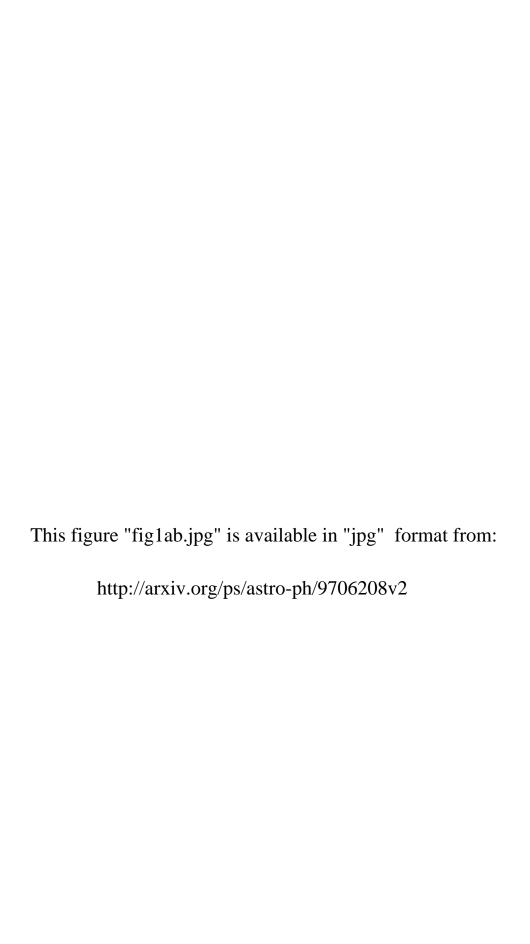
<sup>&</sup>lt;sup>e</sup>The end time is expressed in terms of collision time  $\tau_{coll}$ , and represents the total time from the beginning of the collision.

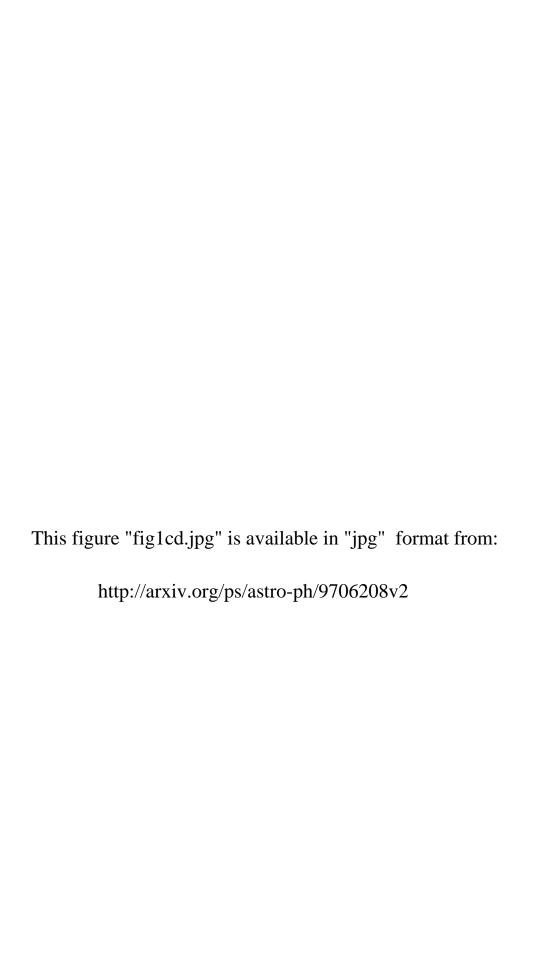
# FIGURE CAPTIONS

- Fig. 1.— Inverted grayscale images of  $\tanh(\log(\rho))$  for Case 1; vector display of the velocity field superimposed. Panel (a) (top) shows the compression phase at  $t = 1.5 \tau_{coll}$  with outflow at the side of the contact discontinuity. Panel (b) (bottom) shows the re-expansion phase at 8.2  $\tau_{coll}$ , with the formation of a dense shell-like structure. Panels (c) and (d) correspond respectively to the collapse phase at  $t = 37.5 \tau_{coll}$  and to the dispersal phase at  $t = 67.5 \tau_{coll}$ . The dramatic development of KHIs and RTIs is evident.
- Fig. 2.— Cut through the grid along the x-axis (y=0.3 $R_c$ ) for Case 1. The top and bottom panel show log-plot of density and pressure respectively. Solid lines refer to  $t = 1.5 \tau_{coll}$ , dot lines to  $t = 8.2 \tau_{coll}$ , short-dash lines to  $t = 37.5 \tau_{coll}$  and long-dash lines to  $t = 67.5 \tau_{coll}$ .
- Fig. 3.— Same grayscale as in Fig. 1, but for Case 2. (a) (top) The compression phase at  $t = 1.5 \tau_{coll}$ , and the ejection of material along the collision plane of the crushed clouds. (b) (center) The re-expansion phase at  $t = 3.7 \tau_{coll}$ ; the (slab) jet-like structure is well-formed and is showing features common to astrophysical jets. (c) (bottom) The structure at  $t = 37.5 \tau_{coll}$ , when the two clouds have merged into a structure with a dense rim. By this time KHI structures are evident along the jet and on the perimeter of the merged cloud.
- Fig. 4.— Same grayscale as in Fig. 1, but now for Case 3. (a) Conditions when the bow shocks generated by the clouds osculate, just prior to impact. (b) The two clouds a little before the actual cloud-body collision. The clouds have been compressed by the bow shocks. (c) The re-expansion phase at  $t = 11.2 \tau_{coll}$ . The two clouds are still distinguishable; also a low density layer has formed around them and is undergoing strong ablation by KHIs.
- Fig. 5.— Same grayscale as in Fig. 1, but now for Case 4, with velocity vectors superimposed. This image shows the final stage of the re-expansion at  $t = 22.5 \tau_{coll}$ . The two clouds have merged into a new structure with density decreasing from the bottom to the top. Delicate density features have been produced by KHIs, enhanced by in flowing wake material deflected along the sides of the clouds.
- Fig. 6.— Same grayscale as in Fig. 1, but now for Case 5, with velocity vectors superimposed. This image shows the complicated re-expansion phase at  $t = 8.2 \tau_{coll}$ . The cloud originating on the left (C1) is still recognizable, whereas C2, coming from the right, has been strongly distorted from its original form.
- Fig. 7.— Same grayscale as in Fig. 1, but now for Case 6. (a) The compression phase at t=3.7  $\tau_{coll}$ . The contact surface is quite irregular and asymmetric, foretelling of the disruption to follow. (b) The structure at t=9  $\tau_{coll}$  showing the formation of a cloudlet breaking off from C1. (c) Density with superimposed velocity vectors, representing the re-expansion phase at t=30  $\tau_{coll}$ . A large irregular structure has formed and eddies are shredding the top part.

Fig. 8.— The four panels show plots of the kinetic energy (a - top left), thermal energy (b - bottom left), center of mass X-cm (c - top right) and Y-cm coordinates (d - bottom right), as a function of time, for each cloud involved in the collision. For Cases 1 and 3 the two colliding clouds are identical to each other, so only one is displayed in each case. Solid lines correspond to Case 1, dotted lines to Case 3, short-dash lines and dot-long dash respectively to cloud C1 (left) and C2 (right) in Case 5. The delay of the features of Cases 3 and 5 with respect to the non-evolved Case 1, is due to the delay in the former cases between impact of bow shocks and cloud bodies.

Fig. 9.— Same as in Fig. 8, but now solid lines refer to Case 2, dot lines to Case 4, short-dash lines and dot-long dash respectively to cloud C1 (left) and C2 (right) in Case 6. Taking care to note the significant difference in the Y-axis scale, A comparison with panels (a) and (b) of Fig. 8 shows that in the radiative cases much less kinetic energy is converted into thermal form. In addition, as shown by the  $X_{cm}$  and  $Y_{cm}$  panels ((c) and (d) respectively) and the significant difference in the y-axis scales of the two figures, re-expansion is much reduced.





This figure "fig2.jpg" is available in "jpg" format from:

This figure "fig3.jpg" is available in "jpg" format from:

This figure "fig4.jpg" is available in "jpg" format from:

This figure "fig5.jpg" is available in "jpg" format from:

This figure "fig6.jpg" is available in "jpg" format from:

This figure "fig7.jpg" is available in "jpg" format from:

This figure "fig8.jpg" is available in "jpg" format from:

This figure "fig9.jpg" is available in "jpg" format from: